SAND2020-0899C

Electrodeposition of nanostructured nickel foils

Alan F. Jankowski

Sandia National Laboratories, P.O. Box 969, Livermore, CA 94551-0969

Abstract

There are many synthesis methods through phase space to produce nanostructures in metals. Condensation methods with rapid solidification are extensively explored from the gas or liquid phase. In particular, electrodeposition using pulsed currents favors continuous nucleation in the processing of structures to produce free-standing sheets as well as protective coatings for surfaces. An analysis approach used to develop the method for refining the structure and surface finish for nanocrystalline gold-copper alloy coatings relates the energy in each deposition pulse to the constituent grain size that forms during growth. Application is now pursued to evaluate a predetermination of the grain size of nanocrystalline nickel foils formed by pulsed electrodeposition.

Keywords: pulsed-current; electrodeposition; nanocrystalline; nickel

Introduction

The synthesis of nanostructured materials through powder precursors has been pursued [1] through processing of solids by severe plastic deformation methods such as equal-channel angular pressing/extrusion, and cryogenic milling. In addition, the synthesis of nanostructures can be accomplished through the vapor phase by sputtering, and through the liquid phase – as by

direct- and pulsed- current electrodeposition methods [2-6]. A vapor or aqueous route is advantageous in engineering applications where improvements are desired for wear resistance and environmental corrosion protection. The strength σ of metals and alloys can increase with the strain rate $\dot{\varepsilon}$ under deformation as dependent upon the characteristic length scale h and the operative deformation mechanism. Nanoscale length features of interest for strengthening include grain boundaries, and the spacing of twin boundaries. For a strain rate $\dot{\varepsilon}$ up to ~10^{+2} s^{-1} it can be considered that plastic deformation is dominated by the effects of solute concentration and dislocation motion. Here, the strength σ of nanocrystalline materials is greater than microcrystalline counterparts in accordance with Hall-Petch type behavior. For grain size values below ~10 nm, as Hall-Petch behavior ceases, plastic deformation transitions to the sliding and rotation of grain boundaries. For a strain rate $\dot{\varepsilon}$ beyond 10^2 s^{-1}, the effect of phonon drag on dislocation motion is reviewed [7] to rapidly increase strength for microcrystalline metals. For even higher strain rates, the effects of length scale should diminish as well. The mechanical strength measurements are accomplished through conventional tension testing, Vickers microhardness, and tribo-indentation (for $\dot{\varepsilon}$ >10^{-1} s^{-1}). The increase in the strain-rate sensitivity of strength exponent m is reported [8] for nanocrystalline and microcrystalline nickel Ni structures from lower to higher $\dot{\varepsilon}$. The effect of grain size on strength in nickel is further assessed to explore its role in the transition from low-to-high strain rate behavior. The deposition conditions to produce nanocrystalline deposits of pure nickel are reviewed with the mechanical properties as dependent on grain size and strain rate. The importance of designing structures with controlled nanocrystalline grain size is, therefore, of importance motivating the evaluation of the analytic model for pulsed electrodeposition of nanocrystalline Ni.

Experimental

Synthesis

The solution chemistry used for the nickel electroplating experiments [4, 9] is 240 $g \cdot l^{-1}$ Ni-sulfate, 6 $g \cdot l^{-1}$ Ni-chloride, and 30 $g \cdot l^{-1}$ Boric acid. The 4.0-4.4 pH solution is heated to 60 ºC and agitated with 27.6 KPa (4 psi) bubbling N_2 to ensure mixing. The solution volume is 1.8-3.8 liters. The electrodeposition current is applied in the direct or pulsed modes. The on/off pulse times t_p (s) and measured current density j ($mA \cdot cm^{-2}$) are listed in Table 1 where the total deposition time is typically 30-180 m. For direct current conditions, the off-pulse time is zero. A 2.54 cm anode-to-cathode separation is used where the substrate is a 5 cm wide x 5 cm high x 0.10 mm thick sheet of 0.994 pure iron Fe. A sputter-deposited coating of a 0.9995 pure copper Cu coating serves as a 2 μm release layer for removal of the electrodeposited Ni coating from the substrate sheet. The Ni coating is deposited to a typical thickness that is 50-100 μm, and can be as thick as 250 μm. The addition of 10 $g \cdot l^{-1}$ saccharin is used for some deposits to assess its' effect as a catalyst to promote grain refinement. In general, grain sizes below 50 nm can be produced by the pulsed electrodeposition method.

Structure and strength

The method of x-ray diffraction with a monochromatic wavelength $\lambda_{x\text{-}ray}$ in the $\theta/2\theta$ mode is used to determine the crystallite size h_g as based on a Debye-Scherrer peak broadening analysis [10-12]. The full-width B at half the maximum intensity is used to determine the corrected value B_c for the Bragg reflection with the measured B_m and instrument broadening B_i. A typical B_i-value is 0.20° using the (200) Bragg reflection for the experiments performed with a Rigaku Miniflex diffractometer equipped with a graphite monochromator and Cu k_α radiation.

The crystallite size h_x is used as the means to evaluate the grain size h_g in the analysis of electrodeposition growth kinetics as

$$h_x = 0.94 \cdot \lambda_{x\text{-}ray} \cdot (B_c \cdot \cos\theta)^{-1} \quad (1)$$

$$B_m^2 = B_c^2 + B_i^2 \quad (1)$$

The use of Vickers microhardness and tribo-indentation provide test methods for measuring the surface- and scratch- hardness of the electrodeposits. Vickers microhardness H_v measurements are conducted using a 10 g load. The mechanical test methods to measure strength σ as a function of strain rate $\dot{\varepsilon}$ are the uniaxial tensile and scratch indentation tests. The tensile tests were conducted [8] for $\dot{\varepsilon} < 10^{-1}$ s^{-1} where the σ is measured at the proportional limit, in order to reduce the effects of strain hardening on the measure of strength beyond the initial yield point. The scratch indentation tests were conducted [8, 10] for $\dot{\varepsilon} > 10^{-1}$ s^{-1} where the $\dot{\varepsilon}$ is computed as the scratch indent velocity divided by the scratch indent width. The strain-rate $\dot{\varepsilon}$ sensitivity exponent m for strength σ is computed using the Dorn relationship as

$$\sigma = \sigma_o \cdot \dot{\varepsilon}^{\,m} \quad (3a)$$

$$m = \partial(\ln \sigma)/\partial(\ln \dot{\varepsilon}) \quad (3b)$$

The samples measured are the electrodeposited nanocrystalline and rolled Ni foils [8]. The equivalent tensile-test value for σ is determined from the scratch indent hardness H_s through use of the von Mises criteria, since the scratch indent test represents a shearing deformation.

Results and Analysis

Four of the electrodeposited samples are used to evaluate effects of using the saccharin catalyst addition and a pulsed current on the nanocrystalline growth morphology. These samples

are listed in Table 1 as direct current no. 30610; 30402*, and pulsed current no. 30611; 30415*, where the asterisk (*) designates the saccharin solute addition to the electrodeposition solution. The samples are listed in the order of increasing current density j.

Table I. Electrodeposition parameters and properties of nickel

Sample	j (mA·cm^{-2})	U (V)	t_p^{on} (ms)	t_p^{off} (ms)	h_g (nm)	H (GPa)
20619	3.0	0.11	15	30	325	-
30312*	9.2	0.41	1.5	3.0	81	-
30401*	9.2	0.42	1.5	3.0	144	-
30415*	9.2	0.43	2.0	4.0	81	3.03
30611	9.2	0.46	2.0	4.0	61	2.69
30311	9.2	0.53	2.0	8.0	34	-
30610	34.8	1.9	1.0	0	50	4.54
30612	34.8	2.5	2.0	0	50	-
30402*	34.8	2.6	1.0	0	35	4.62
30616	47.0	1.7	1.0	0	51	-
20423	57.0	3.2	2.0	0	8	-
20930	124	3.0	2.0	0	47	3.80
21002*	134	3.9	2.0	0	11	6.40

Note: Samples deposited with a saccharin solute are noted with an asterisk (*).

The Ni electrodeposits are metallographically prepared for imaging in cross-section, as shown in Fig. 1, where the growth direction is from bottom to top. In general, the Fig. 1 images reveal a columnar growth with a finer grain and subgrain crystallite structure. The surface finish of the Fig. 1 deposits using the catalyst appear more reflective (although unquantified) than those without. Although the addition of saccharin increases the hardness by up to 10%, the direct current samples appear harder, in general, than the pulsed current counterparts. Anisotropic growth structure that results between these current conditions will need to be evaluated to further resolve the differences in hardness behavior. When comparing results for samples no. 20930 and

21002*), a significant increase in direct current density from <35 to >124 mA·cm^{-2} is found to further increase the hardness by 70% from 3.8 to 6.4 GPa for the catalyst-assisted deposition. A measure of the crystallite, i.e. grain, size will allow for assessment of the Hall-Petch effect.

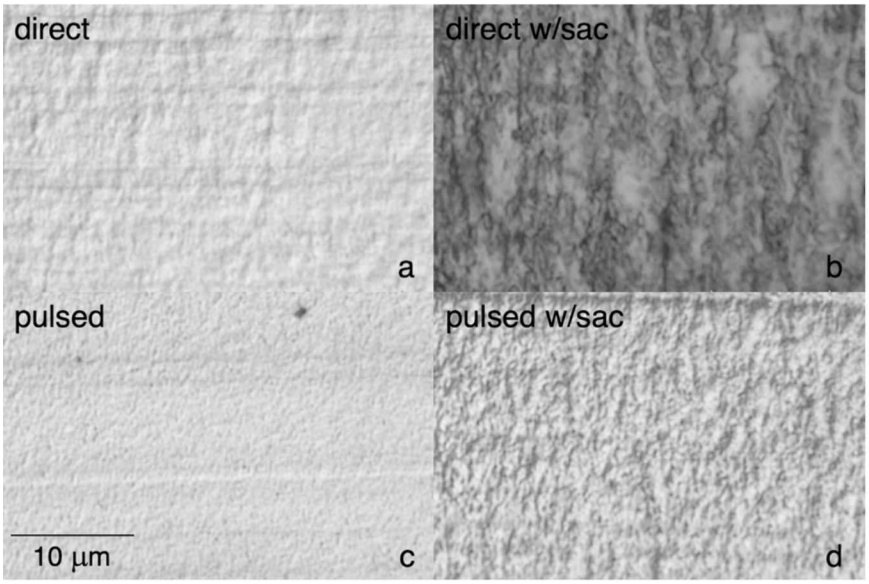

Fig. 1 The Ni coatings are viewed in cross-section as electrodeposited under applied currents that are (a) direct, (b) direct with saccharin, (c) pulsed, and (d) pulsed with saccharin.

The x-ray diffraction scans for representative electrodeposited Ni foils are shown in Fig. 2 along with the results for comparison to a control Ni sample, in this case a rolled foil. The three scans are offset by 2° along the 2θ axis to avoid overlapping the multiple Bragg reflections. The direct-current deposit sample no. 30612 has a strong (200) intensity and is perhaps more anisotropic in its mechanical behavior than the pulsed-current sample no. 30311 which appears to have a more polycrystalline texture. The computations of the crystallite size to represent grain size h_g are made with eqns. 1-2 using the (200) peak broadening measurements. The resulting

computed h_g-values are listed in Table 1. Precision in the grain size is limited to 20% as based on the measurement of peak broadening input to eqns. 1-2.

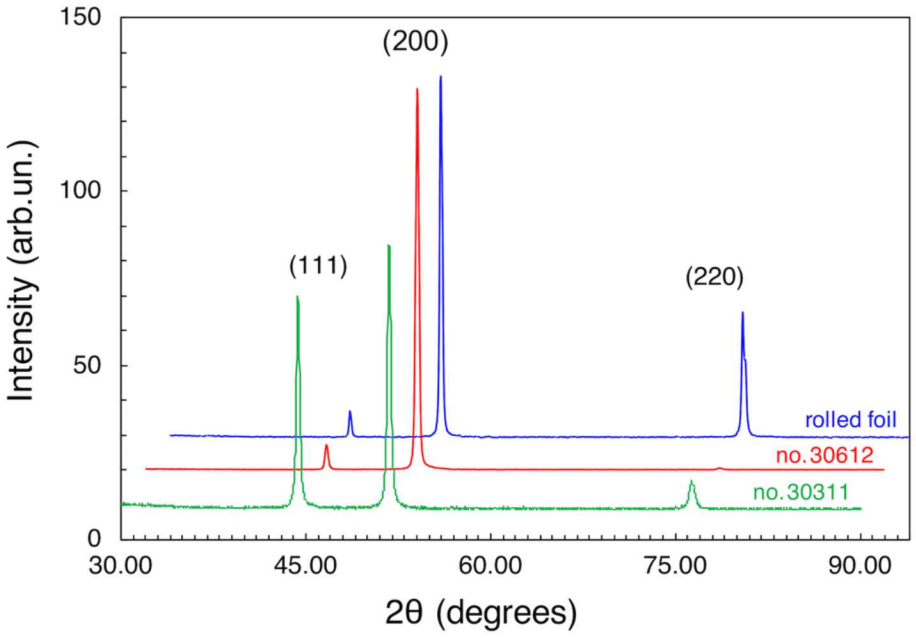

Fig. 2 The x-ray diffraction scans of intensity as a function of 2θ for the electrodeposited samples no. 30311 (pulsed) and 30612 (direct), along with a rolled Ni foil.

The analytic model developed [4, 9] to relate the nanocrystalline grain size with the parameters of the pulsed electrodeposition process is based on Faraday's 1st and 2nd Laws. To review, an expression for the diffusivity D is proposed as based on the on-time for the pulse to produce a nanocrystalline volume at each nucleation site. The energy per pulse Q^* during the electrodeposition process replaces the classic $R \cdot T$ term for energy during diffusion where T is temperature absolute and Q is the activation energy. The diffusivity is proportional to the square of the crystallite size h_g formed during the pulse for its on-time t_p pulse duration. These two relationships are presented in eqns. 4a-4b, correspondingly, as

$$D = D_o \cdot e^{-(Q/Q^*)} \quad (4a)$$

$$D = (h_g^2 \cdot t_p^{-1}) \quad (4b)$$

An expression for the energy per pulse Q^* can be formulated using Faraday's Law, as presented in eqn. 5a, where q is the total charge at a driving potential U. By accounting for the total number of atoms that are transported for the charge during each pulse, an expression [4] for the energy per pulse then follows from eqn. 5a as presented in eqn. 5b, where j is the current density, a_o is the lattice parameter for the crystalline material being deposited, and N_A is Avogadro's number.

$$Q^* = (q \cdot U) \quad (5a)$$

$$Q^* = N_A \cdot (j \cdot t_p \cdot a_o^2) \cdot U \quad (5b)$$

A plot of $(Q^*)^{-1}$ versus D as both values are determined experimentally using eqns. 5b and 4b, respectively, should then produce a straight line where the slope is used to determine the activation energy Q for that deposition condition. Results that are obtained for the short-pulse electrodeposition [4-5] of nanocrystalline Au(Cu) are plotted in Fig. 3 along with new results computed for Ni. The shallow-slope fitted to the pulsed condition of the Au(Cu) results represents the nucleation dominated process with an equivalent activation energy Q equal to only 0.14 ± 0.01 eV·atom^{-1} (13 kJ·mol^{-1}). The Au(Cu) data for pulsed and direct current processes are plotted as peak-values as well, using the duty cycle as a divisor. This time-averaged condition represents the peak values for current density, cell potential, and pulse time. An activation energy of 1.71 ± 0.21 eV·atom^{-1} (165 kJ·mol^{-1}) now results that is representative of the 1.52-1.94 eV·atom^{-1} values reported [9] for long-pulse and peak current Au(Cu) electrodeposition conditions, and is near equivalent to the 1.85 eV·atom^{-1} value for Au^{198} isotope diffusion in a bulk Au(Cu) alloy.

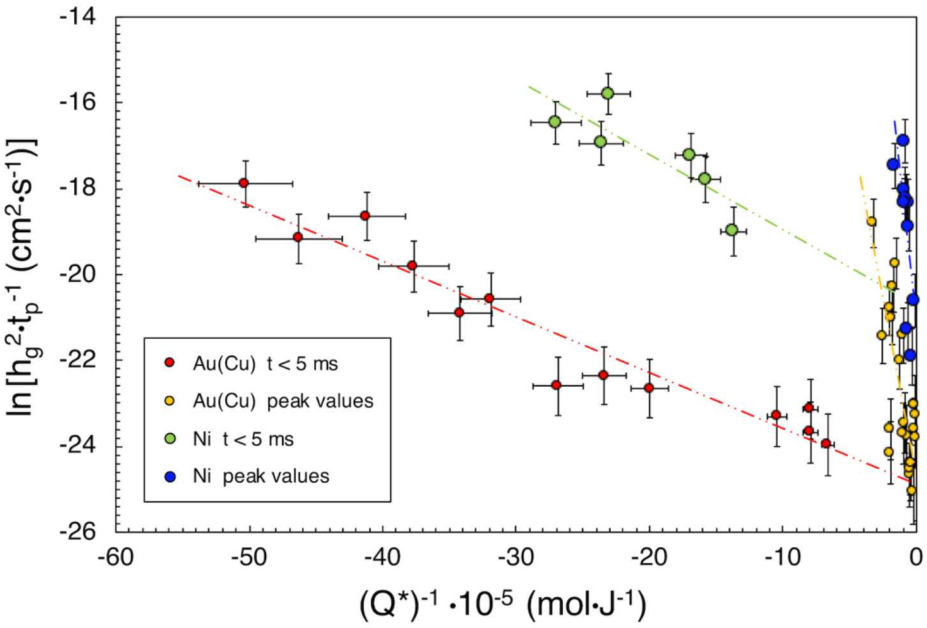

Fig. 3 The variation of $\ln[h_g^2 \cdot t_p^{-1}\ (\mathrm{cm^2 \cdot s^{-1}})]$ with $(Q^*)^{-1}\ (\mathrm{mol \cdot J^{-1}})$ is plotted for the electrodeposited Ni and Au(Cu) samples using direct and short-pulse current conditions.

The results for Ni electrodeposition are plotted in Fig. 3 as well for both the short-pulse, i.e. for on-time pulses t_p less than 5 ms, and the peak-value conditions. The activation energy of 2.93 ± 0.43 eV·atom^{-1} (283 kJ·mol^{-1}) for the time-averaged peak-value curve is near equivalent to the value of 3.04 eV·atom^{-1} (70 kcal·mol^{-1}) as reported [13] for volume or bulk self-diffusion. A short-pulse current value of 0.18 ± 0.05 eV·atom^{-1} (17 kJ·mol^{-1}) for the activation energy is much lower than the bulk value, and even less than the 0.86 eV·atom^{-1} (20 kcal·mol^{-1}) value reported [14] for surface self-diffusion. Once established, the curves for the pulsed and peak current conditions can be used to predetermine h_g for new Q^* conditions. The experimentally determined values obtained for the eqn. 4a parameters of intrinsic diffusivity D_o and Q are listed in Table 2, where the pulsed and peak values for D_o appear to converge for both the Ni and Au(Cu) cases.

Table II. Intrinsic diffusivity D_o and activation energy Q of electrodeposits			
Material	Condition	D_o (10^{-9} cm^2·s^{-1})	Q (eV·atom^{-1})
Ni	pulsed	$(2.1\pm0.9)\cdot10^{-9}$	0.18±0.05
	peak	$(1.8\pm0.7)\cdot10^{-9}$	2.93±0.43
Au(Cu)	pulsed	$(1.6\pm0.5)\cdot10^{-11}$	0.14±0.01
	Peak	$(1.9\pm0.8)\cdot10^{-11}$	1.71±0.21

The results of the Vickers microhardness tests are presented in the Hall-Petch plots of Fig. 4 for the Au(Cu) and Ni electrodeposits. Additional hardness data for Au(Cu), to that reported previously [5], illustrates the loss of Hall-Petch strengthening below a 10 nm grain size. Prior measurements of Ni microhardness for electrodeposited coatings [2] are plotted in Fig. 4 as well for comparison with current Ni results.

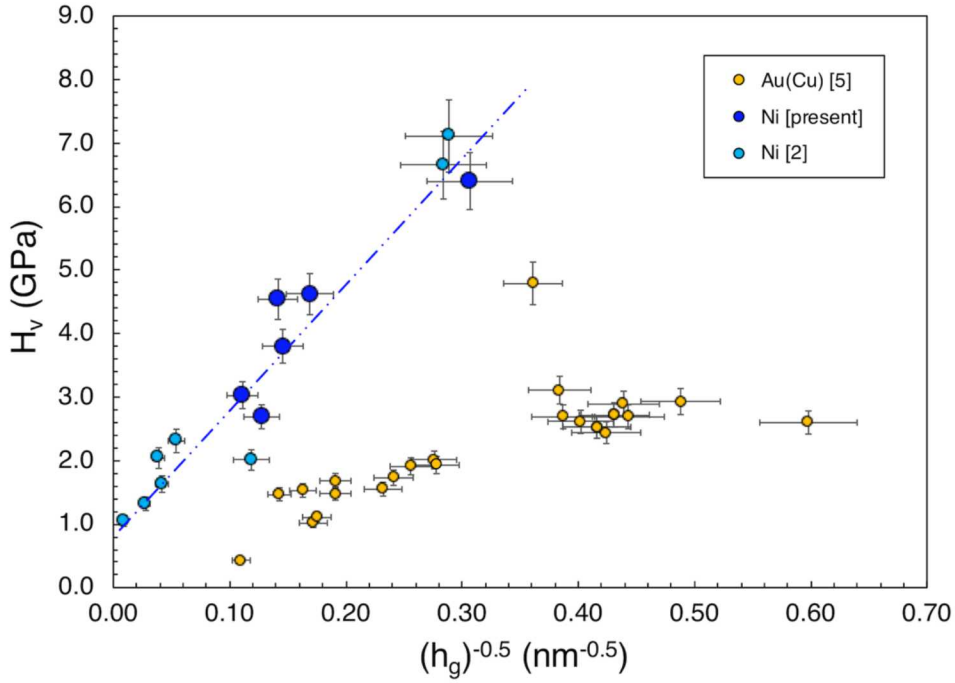

Fig. 4 A Hall-Petch plot of the variation in microhardness H_v (GPa) with inverse-root grain size $h_g^{-0.5}$ ($nm^{-0.5}$) for electrodeposits of Ni and Au(Cu).

The Fig. 5 data plotted for Ni are commensurate between measurement of grain size and microhardness, and correspond with the results of other studies [6] as well. The linear curve for the Ni data can now be used to determine the coefficients in the constitutive equation of the Hall-Petch hardness relationship as

$$H_v = H_o + k_H \cdot h_g^{-0.5} \qquad (6)$$

The intrinsic hardness H_o equals 0.8±0.1 GPa and the hardening coefficient k_H equals 19.8±2.1 GPa·nm$^{0.5}$. The formulation of eqn. 6 is made with respect to grain size measurements as determined using eqn. 1.

The exponent m for the power-law dependence of strength σ on the test strain rate $\dot{\varepsilon}$ is determined from the Fig. 5 data plots using eqn. 3b. There is the appearance of continuity between the tensile test and scratch hardness methods, for determining strength, as a function of increasing strain rate. A best-fit curve analysis, where the correlation coefficient R^2 is >0.92, is used to compute m as made by overlapping the strain-rate and strength data of Fig. 5. These two specific sets of sample data are selected to illustrate several key points regarding the change in strengthening mechanism as a function of $\dot{\varepsilon}$ and h_g. There are two distinct stages observed from the low to high strain-rate, as reported previously [6, 8]. In the present data analysis for the $\dot{\varepsilon}$-range of 10^{-5} – 10^{0} s^{-1}, both the rolled foil and electrodeposit have m-values of 0.063 where the σ_o values for the 26 and 110 nm grain size samples are 1184 and 500 MPa, respectively. For $\dot{\varepsilon}$ >10^{2} s^{-1} data, the m-values increase to 0.154 and 0.162 for the 26 and 110 nm grain size samples, respectively. Although the strength is dependent upon grain size, these results for Ni would suggest that grain size effects on m for Ni are not as significant as found for the Au(Cu) system [10] wherein a large increase in m is observed as grain size decreases below 20-30 nm. In both

Au(Cu) and Ni cases, the larger-grain size samples show a greater strain rate sensitivity for $\dot{\varepsilon}$ $>10^1$ s^{-1}. The Fig. 5 data plots suggest that strength values of the 26 and 110 nm grain size samples will converge at sufficiently high strain rates where the σ_o-values for the higher strain-rate range are 809 and 641 MPa, respectively.

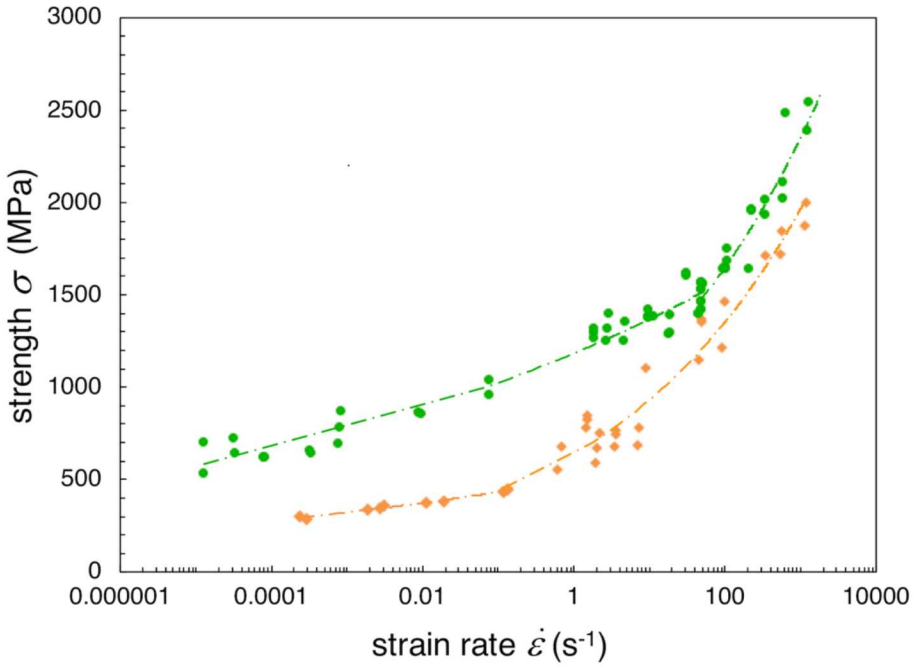

Fig. 5 The strength σ as a function of applied strain rate $\dot{\varepsilon}$ from tensile and scratch hardness measurements for a 26 nm grain-size electrodeposited Ni sample no. 30311 (top curve) , and a 110 nm rolled Ni foil (bottom curve).

Discussion

The data curves plotted in Fig. 3 for both the pulsed and peak current conditions provide values for the intrinsic diffusivity D_o and activation energy Q, as listed in Table 2, that can then be used to estimate the crystallite size in electrodeposits for new growth conditions as defined by the pulse energy Q^* conditions. The peak current conditions represent a convolution of both the

direct current and pulsed current conditions (as normalized using the duty cycle). The instrument hardware used to synthesize the samples by electrodeposition includes program input for the direct current consisting of an on-time and off-time pulse, as listed in Table 1, where the off-time is set to zero. The on-time input was varied between 1 and 2 ms somewhat arbitrarily, where this on-time pulse value is then used in the eqn. 4b-5b computation of D and Q^*, respectively. The effect of the direct current on-time is unclear as the variance that results in the computation of D can't be discerned from the Fig. 3 plots for the Ni and Au(Cu) data, i.e. the plotted values lie within the error bars for the linear curve fits of Q^* versus D.

The measurement of peak broadening from x-ray diffraction to determine crystallite size with eqn. 2 uses an analysis for the convolution of instrument and intrinsic profile that assumes a Gaussian-Gaussian relationship for peak broadening from a mosaic of crystallites as presented in eqn. 1 using the Debye-Scherrer formulation. Limitations to this method exist, and there is often a tendency to underestimate grain size as a result [12] of omitting strain components. For the samples considered in this study, the 2θ position of the (200) Bragg reflection is shifted by less than 0.12° from that of annealed pure nickel, indicating strain effects are quite small (<0.28 %) for these electrodeposits. Similarly, the values computed for grain size are often found to be dependent on the choice of the Bragg reflection. For this reason, the (200) reflection is used as it represents the texture of the direct-current deposits, and is a strong reflection for the more randomly textured pulsed-current deposits. For the (200), the x-ray instrument broadening is calibrated with results for high-resolution image analysis of grain size [15-16] for nanocrystalline Au(Cu) electrodeposits. The limitation to the accuracy of grain size by the x-ray diffraction analysis influences is shown in the error bars for the Ni results as plotted in Figs. 3-4.

The rolled, pure-nickel foil with a 110 nm grain size exhibits a *m*-value of 0.063 in Fig. 4 that is representative of a nanocrystalline solid with dislocation-based strengthening over the strain rate range $10^{-5} < \dot{\varepsilon} < 10^{-1}$ s^{-1}. Similarly, for microcrystalline Ni [6, 17], typical *m*-values are 0.03 or less where the offset method is used to determine yield strength. A transition is seen at higher strain rates as *m* increases to 0.162 for strain rates where $10^{0} < \dot{\varepsilon}$ (s^{-1}) as solute drag effects on dislocation motion enhance strength. The 26 nm electrodeposited-foil sample no. 30311 exhibits the same *m*-value in the lower strain-rate range of $10^{-5} < \dot{\varepsilon} < 10^{2}$ s^{-1} where conventional dislocation motion dominates deformation behavior. Again, at higher strain rates as *m* increases to 0.154 for 10^{2} $s^{-1} < \dot{\varepsilon}$. The increase in *m* at higher strain rates signifies the transition from the range where dislocation behavior dominates the material response to where phonon-drag effects dominate the behavior. Previously, reported data [8] show similar exponents of *m* for the electrodeposited Ni materials in each of the strain-rate ranges of dislocation versus phonon drag based behavior. In comparison, a 5.2 nm grain-size Au(Cu) electrodeposit is of interest since, below ~10 nm, the leveling and loss of Hall-Petch strengthening is reported [10, 16] that may then be associated with an anticipated superplastic-type behavior in nanocrystalline metals [18] that exhibit the deformation mechanisms of grain boundary rotation and sliding at high strain rates. It could be speculated that the smaller number of intragranular dislocations which are found as nanocrystalline grain size is decreased, along with the reduced separation of grain boundaries, reduces the strengthening effect of phonon drag at high $\dot{\varepsilon}$ values.

The effects of nanocrystalline grain refinement in Ni on mechanical strengthening are reported [2, 6] for grain sizes down to 12 nm, where a loss in Hall-Petch strengthening [19] can occur below 10 nm. In an examination of fatigue behavior, the thermal instability [1] of as-deposited nanocrystalline structures are demonstrated for Ni with the evolution of rapid grain

growth upon annealing at low temperature (210 °C) [3] relative to the melt point and a commensurate loss of strength as measured by Vickers microhardness. Just as nanocrystalline Au(Cu) is shown to be temperature sensitive, revealing a low activation energy for grain growth, nanocrystalline Ni is reported to show similar behavior [20] and with evidence reported for dynamic recrystallization under compression [21], although nanocrystalline Ni is generally insensitive to tension, and cyrogenic milling.

Summary

The method of pulsed electrodeposition is used to synthesize nanocrystalline coatings of nickel Ni. The experimental parameters of current density j, cell potential U, and pulse duration t_p are used in a model developed [4, 9] for the electrodeposition process that accounts for the determination of crystallite, i.e. grain, size h_g. The Debye-Scherrer analysis method for line broadening is adequate to estimate h_g from x-ray diffraction scans in the Bragg reflection mode. The electrodeposition process is shown to be dependent on t_p wherein short millisecond pulses produce conditions representative of nucleation dominated growth favoring randomly textured growth with an equivalent activation energy Q of only 0.2 eV·atom^{-1}. Mechanical properties are shown to be consistent with Hall-Petch type behaviors for microhardness with a coefficient k_H of 19.8 GPa·nm$^{0.5}$ and intrinsic hardness H_o of 0.8 GPa. Tensile test and scratch hardness measurements [8] are used to assess strain rate $\dot{\varepsilon}$ sensitivity of strength. An increase in the rate-exponent m to the Dorn relationship from <0.06 to 0.15 is representative of the transition in strengthening mechanism from dislocation-based to phonon drag moderated as $\dot{\varepsilon}$ is increases above 10^2 s^{-1}.

Acknowledgment

Any subjective views or opinions that might be expressed in the paper do not necessarily represent the views of the U.S. Department of Energy or the United States Government. Sandia National Laboratories is a multi-mission laboratory managed and operated by the National Technology and Engineering Solutions of Sandia, LLC., a wholly owned subsidiary of Honeywell International, Inc., for the U.S. Department of Energy's National Nuclear Security Administration under contract DE-NA0003525.

References

[1] C.C. Koch, T.G. Langdon, E.J. Lavernia, “Bulk Nanostructured Materials”, Metall. Mater. Trans. A 48 (2017) 5181-5199.

[2] G.D. Hughes, S.D. Smith, C.S. Pande, H.R. Johnson, R.W. Armstrong, “Hall-Petch strengthening for the microhardness of twelve nanometer grain diameter electrodeposited nickel”, Scripta Mater. 20 (1986) 93-97.

[3] D. Rathmann, M. Marx, C. Motz, “Crack propagation and mechanical properties of electrodeposited nickel with bimodal microstructures in the nanocrystalline and ultrafine grained regime”, J. Mater. Res. 32 (2017) 4573-4582.

[4] A.F. Jankowski, “Modeling Nanocrystalline Grain Growth during the Pulsed Electrodeposition of Gold-Copper”, in Electrodeposition of Nanoengineered Materials, N. Myung, D. Park, R. Penner, and N. Tao (eds.), Electrochemical Society Transactions 1 (12) (2006) 1-9.

[5] A.F. Jankowski, C.K. Saw, J.F. Harper, R.F. Vallier, J.L. Ferreira, and J.P. Hayes, “Nanocrystalline Grain Size Effects in Gold-Copper Electrodeposits”, Thin Solid Films 494 (2006) 268-273.

[6] F. Dalla Torre, H. Van Swygenhoven, M. Victoria, “Nanocrystalline electrodeposited Ni: microstructure and tensile properties”, Acta Mater. 50 (2002) 3957-3970.

[7] J. Harding, “The effect of high strain rate on material properties”, in Materials at High Strain Rates, (ed.) T. Blazynsky (Elsevier Applied Science, Amsterdam, 1987) 136-154.

[8] R.T. Humphrey and A.F. Jankowski, “Strain-Rate Sensitivity of Strength in Macro-to-Micro-to-Nano Crystalline Nickel”, Surface and Coatings Technology 206 (2011) 1846-1849.

[9] A.F. Jankowski, “Diffusion Mechanisms in Nanocrystalline and Nanolaminated Au-Cu”, Defect and Diffusion Forum 266 (2007) 13-28.

[10] L.O. Nyakiti, A.F. Jankowski, “Characterization of strain-rate sensitivity and grain boundary structure in nanocrystalline gold-copper alloys”, Metallurgical and Materials Transactions A 41 (2010) 838-847.

[11] H.P. Klug and L.E. Alexander, X-ray Diffraction Procedures for Polycrystalline and Amorphous Materials, 2nd ed., (John Wiley & Sons, New York, 1974) 618–687.

[12] Z. Zhang, F. Zhou, E.J. Lavernia, “On the Analysis of Grain Size in Bulk Nanocrystalline Materials via X-Ray Diffraction”, Metall. Mater. Trans. A 34 (2003) 1349-1355.

[13] J.R. MacEwan, J.U. MacEwan, and L. Yaffe, “Self-diffusion in Poylcrystalline Nickel”, Canad. J. Chem. 37 (1959) 1623-1628.

[14] A.J. Melmed, “Surface Self-diffusion of Nickel and Platinum”, J. Appl. Phys. 38 (1967) 1885-1892.

[15] L.O. Nyakiti, J. Chaudhuri, and A.F. Jankowski, “High-Resolution Electron Microscopy Characterization of Nanocrystalline Grain Boundaries in Gold-Copper Alloys”, Thin Solid Films 517 (2008) 1182-1185.

[16] A.F. Jankowski and L.O. Nyakiti, “Anomalies in Hall-Petch Strengthening for Nanocrystalline Au-Cu Alloys Below 10 nm Grain Size”, Surface and Coatings Technology 205 (2010) 1398-1402.

[17] M. Chen, E. Ma, and K. Hemker, “Mechanical Behavior of Nanocrystalline Metals”, in Nanomaterials Handbook, (ed.) Y. Gogotsi (Taylor Francis, Boca Raton, 2006) 497-529.

[18] I.A. Ovid’ko, C.S. Pande, R.A. Masumura, “Grain Boundaries in Nanomaterials”, Ch.18 in Nanomaterials Handbook, (ed.) Y. Gogotsi (Taylor Francis, Boa Raton, 2006) 531-552.

[19] A.M. El-Sherik, U. Erb, G. Palumbo, K.T. Aust, “Deviations from Hall–Petch behaviour in as-prepared nanocrystalline nickel”, Scripta Metall. Mater. 27 (1992) 1185-1888.

[20] H. Ni, J. Zhu, Z. Wang, H. Lv, Y. Su, X. Zhang, “A brief overview on grain growth of bulk electrodeposited nanocrystalline nickel and nickel-iron alloys”, Rev. Adv. Mater. Sci. 58 (2019) 98-106.

[21] X. Shen, Z. Xu, J. Lian, Q. Jiang, “The deformation and fracture behavior of an electrodeposited nanocrystalline Ni under compression”, Mater. Sci. Eng’g. A 528 (2011) 7878-7886.